1

2

3

4  **Vps34 PI 3-kinase controls thyroid hormone production by regulating thyroglobulin**

5  **iodination, lysosomal proteolysis and tissue homeostasis**

6

7  Giuseppina Grieco[1*], Tongsong Wang[1*], Ophélie Delcorte[1*], Catherine Spourquet[1*], Virginie

8  Janssens[1], Aurélie Strickaert[2], Héloïse P. Gaide Chevronnay[1], Xiao-Hui Liao[3], Benoît Bilanges[4],

9  Samuel Refetoff[3], Bart Vanhaesebroeck[4], Carine Maenhaut[2], Pierre J. Courtoy[1*], and

10  Christophe E. Pierreux[1*#]

11

12  [1], Cell Biology Unit, de Duve Institute and Université Catholique de Louvain, 1200 Brussels,

13  Belgium;

14  [2], Institute of Interdisciplinary Research (IRIBHM); Université Libre de Bruxelles, 1070 Brussels,

15  Belgium;

16  [3], Departments of Medicine (X-H.L., S.R.) and Pediatrics and Genetics (S.R), The University of

17  Chicago, Chicago, Illinois 60637;

18  [4], UCL Cancer Institute; University College London, 72 Huntley Street, London WC1E 6DD, UK

19

20  [#], correspondence to christophe.pierreux@uclouvain.be

21  *, equal contributions

22

23  Running title: Vps34 controls TH synthesis

24

25     Key words: Vps34, thyroid, hormone, organification, autophagy

26     Dr. Giuseppina Grieco, g.pia@hotmail.it

27     Dr. Tongsong Wang, tswang0802@hotmail.com

28     Ms. Ophélie Delcorte, ophelie.delcorte@uclouvain.be

29     Ms. Catherine Spourquet, catherine.spourquet@uclouvain.be

30     Ms. Virginie Janssens, virginie.janssens@uclouvain.be

31     Dr. Aurélie Strickaert, aurelie.strickaert@ulb.ac.be

32     Dr. Héloïse Gaide-Chevronnay, heloisegaide@hotmail.com

33     Dr. Xia Hui Liao, xliao1@uchicago.edu

34     Dr. Benoit Bilanges, b.bilanges@ucl.ac.uk

35     Prof. Samuel Refetoff, srefetof@uchicago.edu

36     Prof. Bart Vanhaesebroeck, bart.vanh@ucl.ac.uk

37     Prof. Carine Maenhaut, cmaenhau@ulb.ac.be

38     Prof. Pierre J. Courtoy, pierre.courtoy@uclouvain.be

39     Prof. Christophe E. Pierreux, christophe.pierreux@uclouvain.be

40    ***Abstract*** (327 words, 350 allowed)

41

42    **BACKGROUND:** The production of thyroid hormones (T$_3$, T$_4$) depends on the organization of

43    the thyroid in follicles, which are lined by a monolayer of thyrocytes with strict apico-basal

44    polarity. This polarization supports vectorial transport of thyroglobulin for storage into, and

45    recapture from, the colloid. It also allows selective addressing of channels, transporters, ion

46    pumps and enzymes to their appropriate basolateral (NIS, SLC26A7 and Na$^+$/K$^+$-ATPase) or

47    apical membrane domain (Anoctamin, SLC26A4, DUOX2, DUOXA2 and TPO). How these actors

48    of T$_3$/T$_4$ synthesis reach their final destination remains poorly understood. The PI 3-kinase

49    (PI3K) isoform Vps34/PIK3C3 is now recognized as a main component in the general control

50    of vesicular trafficking and of cell homeostasis via the regulation of endosomal trafficking and

51    autophagy. We recently reported that conditional Vps34 inactivation in proximal tubular cells

52    in the kidney prevents normal addressing of apical membrane proteins and causes abortive

53    macroautophagy.

54    **METHODS:** Vps34 was inactivated using a Pax8-driven Cre recombinase system. The impact

55    of Vps34 inactivation in thyrocytes was analyzed by histological, immunolocalization and

56    mRNA expression profiling. Thyroid hormone synthesis was assayed by $^{125}$I injection and

57    serum plasma analysis.

58    **RESULTS:** Vps34$^{cKO}$ mice were born at the expected Mendelian ratio and showed normal

59    growth until postnatal day 14, then stopped growing and died at around 1 month of age. We

60    therefore analyzed thyroid Vps34$^{cKO}$ at postnatal day 14. We found that loss of Vps34 in

61    thyrocytes causes: (i) disorganization of thyroid parenchyma, with abnormal thyrocyte and

62    follicular shape and reduced PAS$^+$ colloidal spaces; (ii) severe non-compensated

63    hypothyroidism with extremely low T$_4$ levels (0.75 ± 0.62 µg/dL) and huge TSH plasma levels

3

64    (19,300 ± 10,500 mU/L); (iii) impaired $^{125}$I organification at comparable uptake and frequent

65    occurrence of follicles with luminal thyroglobulin but non-detectable T4-bearing

66    thyroglobulin; (iv) intense signal in thyrocytes for the lysosomal membrane marker, LAMP-1,

67    as well as thyroglobulin and the autophagy marker, p62, indicating defective lysosomal

68    proteolysis, and (v) presence of macrophages in the colloidal space.

69    **CONCLUSIONS:** We conclude that Vps34 is crucial for thyroid hormonogenesis, at least by

70    controlling epithelial organization, Tg iodination as well as proteolytic $T_3/T_4$ excision in

71    lysosomes.

*Introduction*

72

73      The main function of the thyroid gland is to produce the hormones, $T_3/T_4$ and

74      calcitonin, which are essential for the regulation of metabolic processes (1,2). The production

75      of $T_3$ and $T_4$ depends on the correct tissue organization of thyroid epithelial cells, the

76      thyrocytes, into functional and independent units, the follicles. These are composed of a single

77      layer of polarized thyrocytes that form a spherical structure delineating an internal space or

78      lumen where the thyrocyte secretory product, thyroglobulin, is stored in a colloidal form, thus

79      called the colloid lumen. As thyrocytes communicate via gap junctions, each follicle functions

80      as an integrated unit. Thyroid hormone synthesis depends on apico-basal cell polarity that

81      allows the specific localization of channels, transporters, pumps and enzymes at the

82      appropriate membrane domains. Iodide from the bloodstream freely traverses the

83      fenestrated endothelium of the thyroid capillaries and is taken up into thyrocytes via the

84      basolaterally-localized $Na^+/I^-$ symporter (NIS), thanks to a $Na^+$ gradient generated by the

85      $Na^+/K^+$-ATPase. An alternative basolateral transporter, SLC26A7, has been recently reported

86      to also control iodide uptake, although its role might be indirect (3). Iodide diffuses freely

87      within thyrocytes and is next transported across the apical membrane into the colloid space

88      via apically-localized transporters such as anoctamin or pendrin (SLC26A4). Iodide is then

89      rapidly oxidized into iodine by thyroperoxidase (TPO) located at the apical membrane, in the

90      presence of $H_2O_2$, generated by the DUOX2/DUOXA2 apical membrane complex. Iodine is

91      incorporated into accessible tyrosine residues close to the N- and C-termini of thyroglobulin

92      (Tg), a large protein secreted by thyrocytes into the colloid space. Iodotyrosine rearranges into

93      hormonogenic peptides, which are the direct $T_3$ and $T_4$ precursors. Thyroid hormone synthesis

94      thus requires basal localization of NIS, SLC26A7 and $Na^+/K^+$-ATPase, apical localization of

95      anoctamin, pendrin, TPO, DUOX2 and DUOXA2, as well as apical delivery of Tg into the colloid

96  lumen and endocytic uptake of iodoTg into thyrocyte lysosomes (1,2). Specific regulators of

97  thyroid follicular organization have recently been identified (4). Transcriptomic comparison of

98  thyroid FRT cells cultured in 2D monolayers and in 3D spherical follicles indeed revealed

99  involvement of structural and functional cell elements such as adherens and tight junctions

100  (cadherin-16), cytoskeleton proteins, ions channels, proteins involved in differentiation, and

101  components of the trafficking machinery (e.g. myosin-Vb, Rab17) (4).

102  There is strong evidence that vesicular trafficking is critical for apico-basal polarization

103  and epithelial function (5-7), but the role of vesicular trafficking in thyroid function is

104  incompletely understood. Vps34/*PIK3C3* (also referred to as type III PI3K) has long been

105  recognized as a main actor involved in the general control of endocytic vesicular trafficking (8-

106  13). Vps34/PIK3C3 also plays an important role in epithelial organization in *Drosophila* (14)

107  and in autophagy (12,15), both in the initiation of autophagosome formation and the

108  progression towards autophagosome-lysosome fusion (16,17).

109  We recently inactivated Vps34 in kidney proximal tubular cells (PTC) using Wnt4-Cre

110  and Pax8-Cre (18,19). Wnt4-Cre driven Vps34 excision caused major perinatal lethality, with

111  abnormalities in kidney cortex development and PTC apical differentiation in the surviving

112  mice. With the Pax8-Cre, which triggers recombination in nephrogenic tubules and in

113  nonvascular components of glomeruli two days later than Wnt4-Cre (20,21), we observed

114  normal mouse growth until postnatal (P) day 14 (19). Then, body weight levelled off and all

115  pups died at ~3-5 weeks of age, probably due to kidney failure. Structural and functional

116  studies of Vps34[cKO] kidneys revealed preserved PTC membrane polarity, but impaired apical

117  membrane protein trafficking, thus causing a general PTC dysfunction known as renal Fanconi-

118  like syndrome, manifested by polyuria and low-molecular weight proteinuria. Vps34[cKO] also

119  displayed impaired lysosome size/positioning and blocked autophagy, thereby causing cell

6

120    vacuolization. We concluded that Vps34 is a crucial component of the trafficking machinery

121    necessary for differentiated PTC function and is essential for overall PTC homeostasis (19).

122    Given that Pax8-Cre also triggers recombination in thyrocytes (21), we here investigated the

123    role of Vps34/PIK3C3 in thyroid function and homeostasis.

124    ***Materials and methods***

125    *Mice*

126        Vps34$^{fl/fl}$ mice have been described (22). Pax8-Cre mice were obtained from Dr. M.

127    Busslinger (21). Vps34$^{fl/fl}$ mice were crossed with Pax8-Cre;Vps34$^{fl/+}$ mice to generate

128    conditional targeted excision of Vps34 exon 21 in the thyroid of 25% of offspring (Vps34$^{cKO}$).

129    Non-recombined Vps34$^{fl/fl}$ mice were used as control. Mice were treated according to the NIH

130    Guide for Care and Use of Laboratory Animals, and experiments were approved by the

131    University Animal Welfare Committee, Université Catholique de Louvain (2016/UCL/MD/006

132    and 2018/UCL/MD/026).

133    *Plasma, tissue collection and histology*

134        Blood was collected by eye sinus puncture at sacrifice (P14) under irreversible

135    anesthesia by xylazine 2% and ketamine 50 mg/ml (200  l/mice i.p.). Thyroid lobes were

136    excised, fixed by immersion in neutral-buffered formaldehyde (4% F) at 4°C under stirring

137    overnight. Samples were paraffin-embedded or equilibrated overnight in 20% sucrose and

138    embedded in Tissue-Tek Optimal Cutting Medium (Sakura Finetek) for cryostat sections.

139    *TSH and T4 plasma concentrations*

140    Plasma TSH concentrations were measured by a sensitive, heterologous,

141    disequilibrium double-antibody precipitation RIA as described (23). T4 concentration was

142    measured by coated-tube RIA (Siemens Medical Solution Diagnostics, Los Angeles, CA).

143    *Immunofluorescence*

144    Immunofluorescence was performed on 5 µm-thick frozen sections or on 6 µm-thick

145    paraffin sections (19). Antigen retrieval was promoted in citrate buffer, pH 6.0, at 98°C for 20

146    min using a Lab Vision Pretreatment Module™ (Thermo Scientific). After permeabilization with

147    PBS/0.3% Triton-X100 for 5 min, non-specific sites were blocked by 1-h incubation in PBS/0.3%

148    Triton-X100 with 10% bovine serum albumin (BSA) and 3% milk, followed by primary

149    antibodies (described in Supplementary Table I) in blocking buffer at 4°C overnight. After

150    extensive washing, sections were incubated with the appropriate AlexaFluor-secondary

151    antibodies in 10% BSA/0.3% Triton-X100 at room temperature for 1 h, extensively washed,

152    mounted with Faramount Aqueous Mounting Medium (Dako) and imaged on a spinning disk

153    confocal microscope using a Plan Apochromat 100x/1.4 Oil DIC objective (Cell Observer

154    Spinning Disk; Zeiss). For whole thyroid section recording, images were acquired using Zeiss

155    Pannoramic P250 slide scanner, stitched and analyzed using Case Viewer software.

156    *RT-qPCR*

157    Total RNA was extracted from thyroid lobes using TRIzol Reagent (Thermo Scientific),

158    as described (24). Aliquots of 500 ng RNA were reverse-transcribed by M-MLV reverse

159    transcriptase (Invitrogen) with random hexamers, as described (25). Primer sequences used

160    are described in Supplementary Table II. Real-time qPCR was performed as described (25), in

161    presence of 250 nM of specific primers with Kappa SYBR Fast qPCR Master Mix (Kapa

162    Biosystems) on a CFX96 touch real-time PCR Detection System (Bio-Rad). Data were analyzed

8

163 using the ΔΔCT method, using the geometric mean of *-Actin* and *Rpl27* as reference genes

164 (26).

*$^{125}$I uptake and organification*

166 At postnatal day 8 (P8), mothers and litters were fed with an iodine-free diet for 24 h.

167 At P9, pups were injected intraperitoneally with 1 μCi $^{125}$I (Perkin Elmer) and left for another

168 24 h before sacrifice and thyroid dissection. Both lobes were collected in 2 mM methimazole

169 (Sigma) and homogenized with a glass Potter. Total thyroid $^{125}$I was measured with an

170 automatic gamma counter "Wizard$^2$" (Perkin Elmer) before protein precipitation using 10%

171 trichloroacetic acid (TCA; Merck). After a single wash in TCA, radioactivity was measured in

172 the protein pellet. Percentage of protein-bound iodide was calculated using the ratio of

173 precipitated cpm/total thyroid cpm (27).

*$H_2O_2$ level measurements*

175 The hydrogen peroxide Assay kit from Abcam (ab102500) was used. At P14, thyroid

176 lobes were collected in ice-cold PBS and homogenized with a glass Potter. Proteins were

177 precipitated with perchloric acid 4 M, and supernatant was neutralized with KCl 3 M and KCl

178 1 M until pH was comprised between 6.5 and 8. Fifty l, corresponding to a ninth of a thyroid,

179 was incubated with OxiRed probe and horseradish peroxidase (HRP), according to the

180 instructions form the manufacturer. Fluorescence was measured with a GloMax fluorimeter

181 (Promega, Ex/Em = 535/587 nm).

*Statistical analysis*

183 All statistical analyses were determined by Prism software (GraphPad Software, La

184 Jolla, California, USA). RT-qPCR values were obtained by the ΔΔCT method and are expressed

185    as boxplots with median, 25th and 75th percentiles, and min-max whiskers. Each graph

186    represents the results form a minimum of 8 independent thyroid lobes from at least 3

187    different litters. Nonparametric statistical tests were used: Mann-Whitney for single

188    comparisons. Differences were considered statistically significant when $p<0.05$ (*); ** stands

189    for $p<0.01$; *** for $p<0.001$.

190    **_Results_**

191    _Genetic construction and assessment of Vps34 inactivation_

192        Ubiquitous Vps34 inactivation is embryonically lethal, with embryos dying around

193    embryonic day E8.5 (28). To study tissue-specific roles of Vps34 _in vivo,_ we used a mouse line

194    which carries a floxed _Vps34_ allele (Vps34$^{fl}$) that allows to conditionally delete the loxP-flanked

195    exon 21 of the _Vps34_ gene, which encodes a critical sequence of the lipid kinase domain of

196    Vps34 (22). This approach was designed to allow for the expression of a minimally-truncated,

197    catalytically-inactive    Vps34    protein.    However,    upon    conditional    expression    in

198    megakaryocytes, the level of this truncated Vps34 and its obligatory partner, Vps15, were

199    found to be decreased by 80-90% in the megakaryocyte lineage (thrombocytes), indicating

200    instability of truncated Vps34 protein (22). We will thus hereafter refer to the result of this

201    Vps34 truncation as Vps34 conditional knock-out (Vps34$^{cKO}$).

202        We crossed homozygous Vps34$^{fl/fl}$ mice with Pax8-Cre;Vps34$^{fl/+}$ mice, which is expected

203    to lead to a tissue-specific (thyroid and kidney) conditional excision of exon 21 from both

204    Vps34 alleles in 25% of the pups, which are further referred to as Vps34$^{cKO}$ mice. Vps34$^{cKO}$

205    mice were born at the expected Mendelian ratio and showed normal development until

206    postnatal day 14 (P14), then stopped growing and died at around 1 month of age (19). We

207   therefore analyzed the thyroid of Vps34cKO mice at P14. Of note, eye opening, a marker of

208   cerebral maturation was usually delayed till P10.

209        We first assessed the extent of Vps34 genetic excision in the thyroid by quantification

210   of *Vps34* mRNA using primer that are specific for the total *Vps34* or are exon 21-specific.

211   Compared to control littermate pups, we found a ~70 % reduction of exon 21-containing

212   *Vps34* mRNA in cKO thyroid extracts. In comparison, we found no significant difference in the

213   abundance of *Vps34* mRNA containing exon 22-24 (Fig. 1A). Assuming that *Vps34* is equally

214   expressed in all thyroid cell types (expressing and non-expressing the Cre recombinase), this

215   ~70 % decrease suggests that most thyrocytes in Vps34cKO mice had undergone Cre-mediated

216   recombination.

217   *Vps34cKO thyroids show signs of hyperstimulation by thyroid stimulating hormone (TSH)*

218        At P14, thyroid glands from Vps34cKO were almost twice heavier as compared to

219   control glands (Fig. 1B). Histological staining using Periodic-Acid-Schiff (PAS, which in the

220   thyroid reflects production of the thyroglobulin glycoprotein) readily revealed striking

221   differences between thyroid glands of control and Vps34cKO mice (Fig. 1C). Thyroid glands of

222   control mice appeared as assemblies of round follicular sections of variable diameter, filled

223   with colloid intensely and homogenously stained by PAS. Although histology of Vps34cKO was

224   more variable, the three representative individual thyroids shown in Fig. 1C revealed irregular

225   follicle shape, especially at the periphery of the gland, and weaker or absent PAS staining (Fig.

226   1C and Suppl. Fig. 1). In addition, the PAS-negative follicular space were often filled with nuclei

227   (see Vps34cKO #3). Quantification revealed that 90% of control follicles had a regular shape

228   and intense (+++) PAS staining (Suppl. Fig. 1). On the contrary, only 50% of Vps34cKO follicles

229   displayed a regular shape and most of the follicles were weakly positive for PAS (++ or +)

230    (Suppl. Fig. 1). In addition, 10 to 50% of the Vps34$^{cKO}$ follicles showed no PAS staining (-) and

231    luminal cells were found in 40-70% of the follicles (Suppl. Fig. 1). Confocal

232    immunofluorescence microscopy for the epithelial marker E-cadherin confirmed

233    heterogeneity of Vps34$^{cKO}$ follicles, but also of thyrocytes. Hoechst labelling revealed the

234    presence of several nuclei in a significant fraction of lumina (Fig. 1D). These histological

235    features of follicle remodelling and colloid consumption up to exhaustion, suggested

236    perturbed thyroid function.

237    *Vps34$^{cKO}$ causes severe non-compensated hypothyroidism*

238    To directly test the hypothesis that Vps34$^{cKO}$ could impair thyroid hormone production,

239    plasma was collected at P14 and analyzed for the levels of $T_4$ and TSH. In P14 control pups,

240    values were 6.4 ± 1.5 µg/dL for $T_4$, and 75 ± 110 mU/L for TSH (Fig. 2). In Vps34$^{cKO}$ mice, we

241    found extremely low $T_4$ values (0.75 ± 0.62 µg/dL) and very high plasma levels of TSH (19,311

242    ± 10,482 mU/L) (Fig. 2). These data indicate severe, non-compensated hypothyroidism. This

243    observation, compatible with the growth retardation observed after P15 (19), could be

244    explained by mislocalization of one or several basolateral and/or apical actors involved in

245    thyroid hormone synthesis, as we reported in Vps34$^{cKO}$ kidney proximal tubular cells (19).

246    *Vps34 cKO display reduced iodine organification*

247    The reduced or absent PAS staining (Fig. 1C) and the low $T_4$ plasma levels in Vps34$^{cKO}$

248    mice (Fig. 2) might be caused by defective basolateral iodine uptake, apical transport and/or

249    apical organification on thyroglobulin. Due to lack or very poor specificity of antibodies

250    directed against murine proteins involved in these processes, we first measured their mRNA

251    expression levels in total thyroids at P14 (Fig. 3). We observed no change in mRNA expression

252    of *Nis*, *Ano1*, *Tg*, *Tpo* and *Duox2,* a significant increase in *Tshr* and *Slc26a4* expression, and a

253    significant decrease of *Slc26a7* and *Duoxa2* mRNA levels. At this stage, we cannot conclude if

254    these changes contribute to the observed hypothyroidism of Vps34$^{cKO}$.

255         To further test whether basolateral NIS and SLC26A7 and apical ANO1, SLC26A4, TPO,

256    DUOX and DUOXA were all correctly localized, we functionally assayed their combined activity

257    by injecting iodine-deprived pups at P9 with $^{125}$I. At P10, 24-h post-injection, thyroid lobes

258    were collected and radioactivity measured before and after protein precipitation by TCA (Fig.

259    4A). $^{125}$I uptake was not statistically-different in Vps34$^{cKO}$ and the three control genotypes (Fig.

260    4A), suggesting normal NIS and SLC26A7 function and thus basolateral localization. In marked

261    contrast, only 10% of thyroid $^{125}$I was bound to proteins in Vps34$^{cKO}$ compared to

262    approximately 55% in control genotypes at this stage (Fig. 4A). This indicates a major effect of

263    Vps34 on one or several apical proteins involved in iodine organification.

264         Normal *Ano1* and increased *Slc26a4/Pendrin* mRNA levels suggested correct, or even

265    improved, transfer of iodine in the follicular lumen. On the other hand, decreased *Duoxa2*

266    might impact on $H_2O_2$ production. We thus measured the production of $H_2O_2$ in control and

267    Vps34$^{cKO}$ thyroid lobes. Surprisingly, the median level of $H_2O_2$ production in Vps34$^{cKO}$ was

268    higher, even if we observed variability (Fig. 4B), indicating that the DUOX/DUOXA pair is

269    functional in Vps34$^{cKO}$ thyroid. Altogether, these results suggest defective localization of one

270    or several apical actors involved in iodine organification.

271    *Apical polarity is impaired in Vps34$^{cKO}$*

272         Apico-basal polarity is essential for thyrocyte function and defects in polarity might

273    impact on the delivery, and thus localization, of actors involved in thyroid hormone synthesis.

274    As general markers to assess polarity, we used the basement membrane protein laminin, the

275    basolateral Na$^+$/K$^+$-ATPase, E-cadherin and  -catenin, the apically-localized ERM family

13

276    member ezrin and the tight junction-associated protein ZO-1. Control thyrocytes displayed a

277    well-defined apico-basal polarity with laminin assembled on the basal side, with $Na^+/K^+$-

278    ATPase, E-cadherin and  -catenin restricted to the basolateral membrane and separated from

279    apical ezrin by the tight junction, visualized by ZO-1 (Fig. 5A and 5B). In Vps34$^{cKO}$ thyrocytes,

280    basal laminin was correctly assembled and $Na^+/K^+$-ATPase, E-cadherin and  -catenin were

281    restricted to the basolateral membrane, indicating the presence of functional tight junctions.

282    However, on the apical side of Vps34$^{cKO}$ thyrocytes, the ezrin signal was weaker or absent from

283    the lumen-facing pole of some thyrocytes (Fig. 5A), and most cells also lacked ZO-1 protein

284    labelling (Fig. 5B). These data suggest impaired apical polarity in Vps34$^{cKO}$, which might

285    contribute to defective localization of apical actors involved in iodine organification.

286    *Vps34$^{cKO}$ mice display defective thyroglobulin iodination*

287         To further analyse the significance of the lack of PAS staining in a fraction of Vps34$^{cKO}$

288    follicles (Fig. 1C) and the defect in iodine organification (Fig. 4), we assessed thyroglobulin

289    protein expression and its associated $T_4$ hormonogenic peptide (I-Tg) by immunofluorescence.

290    Low magnification of control sections showed an identical distribution pattern of

291    thyroglobulin and I-Tg, homogeneously filling all round colloidal spaces (Fig. 6A). In Vps34$^{cKO}$,

292    the thyroglobulin labelling was more heterogeneous, mainly due to the presence of cells in

293    the colloid. Remarkably, antibodies recognizing the $T_4$ hormonogenic peptide often failed to

294    label colloidal spaces even when containing Tg in the adjacent section (Fig. 6A), thereby

295    confirming the organification defect (Fig. 4A). Quantification revealed that only a quarter (25.2

296    ± 11.9 %) of the follicles were labeled for $T_4$ hormonogenic peptide. Of specific interest,

297    whereas the Tg signal was restricted to the follicle lumen in control thyroid, high magnification

298    revealed that the Tg signal was frequently seen within Vps34$^{cKO}$ thyrocytes (Fig. 6B,

14

299     arrowheads). These observations indicated that Vps34 deletion caused defective

300     thyroglobulin iodination, as well as reduced Tg exocytosis and/or excessive Tg endocytosis.

301     *Impaired lysosomal function and I-Tg proteolysis in Vps34$^{cKO}$ thyroid*

302             Vps34 is involved in endocytic trafficking and cKO of Vps34 in postnatal kidney

303     glomeruli podocytes causes a strong increase of the overall immunofluorescence signal for

304     the lysosomal membrane marker LAMP-1, indicating enhanced lysosome biogenesis (29,30).

305     We further reported that absence of Vps34 in kidney PTCs causes an increase in the actual

306     size of lysosomes, that were sometimes enlarged, and mislocalized toward the basal pole of

307     the cell (19). Given that lysosomal proteases in thyrocytes are important to excise

308     hormonogenic peptides to release free T$_3$ and T$_4$, we investigated LAMP-1-labeled structures

309     in Vps34$^{cKO}$ thyrocytes as a proxy for lysosomal function, and its co-localization with Tg and I-

310     Tg to demonstrate endocytosis. In our conditions, immunofluorescence on control thyroid

311     sections only produced a weak LAMP-1 signal in the E-cadherin-positive epithelial thyrocytes

312     (Fig. 7A and 7B). On the contrary, a strong and widespread LAMP-1 signal was observed in all

313     Vps34$^{cKO}$ thyrocytes. As shown in the enlarged boxes of Fig. 7A and 7B (separate emission

314     channels in white), LAMP-1-positive late endosomes/lysosomes were more abundant, and

315     sometimes enlarged in Vps34$^{cKO}$ thyrocytes as compared to control. In addition, the

316     intracellular Tg protein, found in most Vps34$^{cKO}$ thyrocytes (Fig. 7A, arrowheads), most often

317     colocalized with LAMP-1-positive structures. This indicates that colloidal Tg was endocytosed

318     by thyrocytes, but that trafficking to or Tg proteolysis within the lysosomes was slower or

319     impaired, as compared to controls. Of note, luminal cells also contained LAMP-1 structures

320     positive for Tg (Fig. 7A, right).

15

321    Additional supporting evidence for impaired lysosomal proteolysis came from the

322    analysis of I-Tg (Fig. 7B). Indeed, Vps34$^{cKO}$ thyrocytes often contained intracellular signal for I-

323    Tg, colocalizing within LAMP-1 structures (Fig. 7B, enlarged boxes,). Thus, in addition to

324    reduced iodine organification, defective lysosomal proteolysis of $T_3/T_4$, if/when hormonogenic

325    peptides were still formed on Tg, was also accounting for the low $T_3/T_4$ plasma levels observed

326    in Vps34$^{cKO}$ (Fig. 2).

327    *Evaluation of autophagy in Vps34$^{cKO}$ thyroid*

328    The deletion of Vps34 in the kidney also causes a block of autophagy (19). We therefore

329    assessed the expression of p62 (also called sequestosome-1, or SQSTM1), a polyubiquitin-

330    binding protein that interacts with LC3b (microtubule associated protein 1 light chain) on the

331    autophagosome membrane and is normally continuously degraded by the autophagy process

332    (31). Since p62 accumulates when completion of autophagy is inhibited, p62 can be used as a

333    marker to study autophagic flux (32). Although we found a weak punctiform LC3 signal in

334    control thyrocytes, we observed no p62 signal, indicating normal autophagic flux in control

335    thyroid. As reported, few LAMP-1-labelled structures were found in control thyroid. In

336    contrast, much larger structures, mostly double-labeled for p62 and LC3, were easily detected

337    in the cytoplasm of Vps34$^{cKO}$ thyrocytes. As the LAMP-1 signal was increased in Vps34$^{cKO}$, these

338    p62/LC3-positive punctae sometimes co-localized with LAMP-1. We concluded that LC3 could

339    be recruited on p62 aggregates but that progression to autophagosome maturation and fusion

340    with, and degradation by, lysosomes was arrested. This suggested that deletion of Vps34 in

341    thyrocytes abrogated the autophagic flux.

342    Recent evidences have demonstrated that p62 is also an activator of the antioxidant

343    KEAP1/NRF2 pathway, which impacts on thyrocyte physiology and Tg biology (33). We thus

344    examined the possibility that stabilized p62 would compete with NRF2 for KEAP1 binding in

345    Vps34$^{cKO}$, thus allowing NRF2 to reach the nucleus and activate gene expression. We

346    quantified the mRNA levels of *Nrf2* and its target genes *Nqo1*, *Gpx2* and *Txnrd1*. Although we

347    measured a slight decrease of *Nrf2* mRNA in Vps34$^{cKO}$, two of its target genes, namely the

348    quinone reductase, *Nqo1*, and the thioredoxin reductase 1, *Txnrd1*, were upregulated 1.9- and

349    3.5-fold, respectively (Fig. 8B). This observation supports the hypothesis that KEAP1

350    interaction with p62 is favored in Vps34$^{cKO}$ and that NRF2 is thus displaced and able to migrate

351    to the nucleus to regulate gene expression.

352         We also evaluated macroautophagy/mitophagy by immunolocalizing TOM20 and

353    LAMP-1. In Vps34$^{cKO}$ thyrocytes, TOM20-labeled structures did not colocalize with the more

354    abundant, enlarged LAMP-1+ structures (Suppl. Fig. 2A), as we also reported in Vps34$^{cKO}$

355    kidney proximal tubular cells (19). This suggested that sequestration of mitochondria into

356    autophagosomes is either not triggered, which is unlikely for altered cells, or abortive at P14

357    in Vps34$^{cKO}$ thyrocytes, and/or that fusion of autophagosomes with lysosomes is prevented.

358    We then evaluated the chaperone-mediated autophagy by immunolocalizing LAMP-2A. As

359    compared to control thyroid, LAMP-2A-labeled structures were more abundant in Vps34$^{cKO}$

360    thyrocytes (Suppl. Fig. 2B), as we also reported in Vps34$^{cKO}$ kidney proximal tubular cells (19).

361    *Luminal cells present in Vps34$^{cKO}$ follicles are macrophages*

362         Finally, we investigated the origin of the cells present in the colloidal space. As

363    observed in Figure 7A, cells trapped in the follicular lumen showed a strong LAMP-1 signal

364    (Fig. 7A). However, they were negative for E-cadherin (Figs. 1D and 5A). In addition, we found

365    that luminal cells were also negative for the permanently-expressed thyrocyte-specific

366    transcription factor, TTF-1 (Fig. 9A), indicating that these cells were not derived from the

17

367 thyrocyte lineage. Lineage-tracing experiments on Pax8-Cre; Vps34$^{fl/fl}$;ROSA-STOP-YFP pups at

368 P14 further revealed YFP-positive signal only in follicle-delineating thyrocytes and not in the

369 luminal cells (Fig. 9B). Thus, luminal cells had never expressed Pax8 and were thus not derived

370 from thyrocyte progenitors. Although infiltration by C-cells was a possibilty, we failed to label

371 luminal cells for the Prox1 transcription factor. As luminal cells displayed LAMP-1 signal and

372 were also positive for Tg (Fig. 7A), we tested the possibility that luminal cells were infiltrating

373 macrophages. This was the case: luminal cells were labeled by the macrophage marker F4/80

374 (Fig. 10A), but not by E-cadherin. To confirm that colloid was consumed by infiltrated

375 macrophages, we performed a triple immunolabelling for F4/80, LAMP-1 and I-Tg. Luminal

376 F4/80-positive cells displayed huge LAMP-1-positive lysosomes filled with I-Tg (Fig. 10B). Thus,

377 colloid consumption (Tg in Fig. 7A and I-Tg in Fig. 9D) by infiltrated macrophages provides a

378 third explanation for the low $T_4$ plasma level observed in Vps34$^{cKO}$.


379 *Discussion*


380       In this study, we report that deleting Vps34 in thyrocytes by Pax8-Cre-driven

381 recombination causes several defects in the thyroid: (i) doubling of thyroid weight and

382 perturbed thyroid parenchyma organization, with reduced PAS$^+$ colloidal spaces; (ii) severe

383 hypothyroidism with collapsed plasma $T_4$ levels and very high TSH; (iii) strong decrease of $^{125}$I

384 organification, at comparable $^{125}$I uptake, and of $T_4$ formation on thyroglobulin (detected by

385 immunofluorescence as early as P3); (iv) defective apical polarization; (v) impaired lysosomal

386 proteolysis; (vi) infiltration of macrophages in the colloid. Some of these features, combined

387 with delayed "eye opening" and impaired postnatal growth after two weeks (18), phenocopy

388 the impact of *Duoxa2* KO in the thyroid (34).

389   DUOXA2 is a chaperone protein required for the correct localization of DUOX2 at the

390   apical pole of thyrocyte, where the complex (DUOX2/DUOXA2) produces $H_2O_2$. In the absence

391   of DUOXA2, $H_2O_2$ is not produced and subsequent thyroperoxidase-mediated oxidation of

392   iodide into reactive compounds and thyroglobulin iodination are abolished (34). The similarity

393   of the severity of hypothyroidism in Vps34$^{cKO}$ and *Duoxa2* KO mice prompted us pay a closer

394   look at DUOXA2 in Vps34$^{cKO}$. We found that the expression of *Duoxa2* started decreasing after

395   P3, reaching two-fold lower values at P14. It is interesting to note that expression of *Duox2*

396   and *Duoxa2* mRNAs was quantitatively different, despite of the fact that they share the same

397   promoter (35). Whether decreased *Duoxa2* mRNA expression is reflected by equivalent two-

398   fold decrease of DUOX2/DUOXA2 complex at the apical pole is unknown. However, it is very

399   unlikely that a two-fold decrease would by itself so severely impact on thyroglobulin

400   iodination, since heterozygous mice for *Duoxa2* deletion have virtually no phenotype. In

401   addition, our measurements of $H_2O_2$ levels in total Vps34$^{cKO}$ thyroid extracts also support

402   normal, or increased, function of the DUOX2/DUOXA2 complex. Instead, based on the known

403   functions of Vps34 in kidney PTCs, where its inactivation causes lack of apical localization of

404   endocytic receptors (megalin, cubilin) and solute transporters (NaPi-IIa, SGLT-2) (19), it would

405   be extremely interesting to localize actors of thyroid hormonogenesis on thyroid sections, and

406   assess their basolateral or apical addressing in Vps34$^{cKO}$ thyrocytes. Unfortunately, reliable

407   antibodies to detect most of these proteins are not yet available for mice. Nevertheless, [125]I

408   uptake and processing experiments suggests normal localization and function of the sodium-

409   iodine symporter, NIS, and/or the alternative transporter SLC26A7 (3), and rather support the

410   hypothesis of defective apical localization of one or several actors involved in thyroid

411   hormonogenesis (Ano1, pendrin, TPO, DUOX, DUOXA).

19

412    Characteristic histopathological alterations combined with the very high plasma TSH

413    levels and two-fold increased *Tshr* expression in Vps34$^{cKO}$ thyroid suggest that thyrocytes are

414    in a hyperstimulated state. For example, DuoxA2 KO, which display very high TSH levels,

415    present a 20- and 5-fold higher expression level of *Nis* and *Tpo*, as compared to controls (34).

416    However, the expression of these two sensitive target genes of the TSH signaling pathway, *Nis*

417    and *Tpo*, was surprisingly unchanged in Vps34$^{cKO}$, arguing against thyrocyte hyperstimulation.

418    We favor the hypothesis of TSHR mistrafficking into intracellular vesicles. Recent work in

419    *Drosophila* revealed that Vps34 inactivation or pharmacological inhibition using the small

420    molecule inhibitor, SAR405, caused alteration of cell polarity and disruption of epithelial

421    architecture by relieving LKB1 inhibition and triggering JNK activation (14). A role of Vps34 in

422    epithelial organization and polarity was also observed in 3D cultures of Caco-2 kidney cells

423    (14). It would be interesting to analyze the activation states of LKB1 and JNK in Vps34$^{cKO}$

424    thyroid, and, if modified, to cross Vps34$^{cKO}$ with floxed LKB1 alleles.

425    The expression of the two SLC transporters, *Slc26a7* and *Slc26a4*, came out as a

426    surprise in Vps34$^{cKO}$. Decreased expression of Slc26a7 (4-fold) in Vps34$^{cKO}$ may affect entry of

427    iodine in the thyroid. However, it should be mentioned that this alternative basolateral

428    transporter, SLC26A7, may only play an indirect role on iodine uptake (3). In addition,

429    expression of the main transporter, *Nis*, is at least 16-fold more important than that of

430    *Slc26a7*. This may explain why $^{125}$I uptake was not affected. Expression of apical *Slc26a4*

431    (pendrin) in Vps34$^{cKO}$ was even more dramatic with a 20-fold increase in expression. However,

432    we do not think that this would have affected apical transport of iodine. Indeed, in control

433    thyroids, expression level of *Slc26a4* were 60-fold less important than those of *anoctamin1* (6

434    Ct). This supports a more prominent role for *anoctamin1* in iodine apical transport, as

435    demonstrated by Twyffels (36). These changes in expression of *Slc26a7* and *Slc26a4* could

20

436   however impact on thyrocyte ion balance. Indeed, SLC26A7 and SLC26A4 transporters have

437   opposite action on chloride ions at the basolateral and apical membranes, respectively.

438   Decreased levels of SLC26A7 at the basolateral membrane may decrease the export of

439   chloride out of the thyrocyte (3). On the contrary the increase of SLC26A4 at the apical

440   membrane may increase the entry of chloride in the thyrocyte. Accumulation of chloride may

441   in turn decrease intracellular pH and causes cellular stress in Vps34$^{cKO}$.

442        The weak PAS staining in Vps34$^{cKO}$ could be due to decreased exocytosis of Tg or

443   increased Tg endocytosis. We indeed very often observed intracellular Tg in Vps34$^{cKO}$. We

444   suggest that the defective process is the endocytic route rather than exocytosis because we

445   readily observed intracellular structures positive for iodinated Tg. This is rarely the case in

446   control thyrocyte where I-Tg is rapidly proteolytically processed. In addition, our work also

447   evidenced increased abundance and size of LAMP-1-positive late endosomes/lysosomes in

448   Vps34$^{cKO}$ thyrocytes, with accumulation of Tg and the autophagic marker, p62, indicative of a

449   defective lysosomal trafficking and/or function. In addition to impaired Tg iodination, low $T_4$

450   plasma levels thus also probably result from impaired endocytic transport of iodo-Tg to

451   lysosomes and/or proteolytic excision of $T_3$/$T_4$ therein. Several studies have reported a role

452   for Vps34 in endocytic trafficking to lysosomes (13, 15, 30, 37) and activation of lysosomal

453   proteases (15). In our study on Vps34$^{cKO}$ kidney PTCs, we also observed enlargement of

454   lysosomes and their filling by undigested material, labelled for a variety of antigens (19). In

455   Vps34$^{cKO}$ thyrocytes, we also observed increased abundance and size of LAMP-1-positive

456   compartments filled with Tg and I-Tg. Based on these and previous findings showing that

457   Vps34 deletion leads to late endosome/lysosome enlargement and defective lysosomal

458   function (37), we assume a defective proteolytic excision of $T_3$/$T_4$ from iodo-Tg, analogous to

459   what we reported in cystinotic $Ctns^{-/-}$ mice (38). Cystinosis is a lysosomal storage disease due

460    to deletion or inactivating mutations of the lysosomal cystine transporter, cystinosin (39).

461    Defective cystinosin impacts on lysosomal proteolysis, presumably due to endolysosomal

462    mislocalization, impaired pro-cathepsin maturation and altered luminal redox status;

463    autophagic flux is also altered (40). Like cystinotic patients, $Ctns^{-/-}$ mice show compensated

464    hypothyroidism with moderate increase of TSH, thyrocyte hyperplasia and proliferation,

465    combined with progressive colloid depletion and evidence of increased endocytosis into

466    colloid droplets. Iodo-thyroglobulin could be detected in $Ctns^{-/-}$ but not wild-type thyrocyte

467    lysosomes, under identical labelling conditions, further indicating defective proteolysis.

468         It has recently become clear that Vps34 may act on lysosome positioning, which is

469    crucial to autophagosome formation (41,42). Similar to the kidney PTC defect, we observed

470    an increased p62 signal in Vps34$^{cKO}$ thyroids at P14. Accumulation of p62 and LC3b in Vps34$^{cKO}$

471    indicates a block in the autophagy process. In addition, p62 accumulation also suggests

472    activation of the antioxidant NRF2 pathway by competitive binding of p62 to KEAP1 (33). We

473    indeed observed increased expression of two NRF2 target genes, namely the quinone

474    reductase, $Nqo1$, and the thioredoxin reductase 1, $Txnrd1$. Considering the expected key role

475    of Vps34 in macroautophagy, our data on mitophagy do not prove, but are compatible with

476    the suggestion that this important homeostatic process is abrogated upon Vps34 deficiency.

477         A final observation deserving discussion is the occurrence of viable cells in the follicular

478    lumens of Vps34$^{cKO}$ thyroids. Our first hypothesis was that defective endocytic and autophagic

479    routes to the lysosomes could impact thyrocyte homeostasis, thus causing cellular stress.

480    Cellular stress, induced by defective autophagosome and lysosomal function, or by activation

481    of stress kinase such as JNK, could explain shedding of thyrocytes cells into the colloidal space.

482    However, luminal cells of Vps34$^{cKO}$ thyroids were negative for E-cadherin and the thyrocyte-

483    specific transcription factor, TTF-1. Furthermore, lineage tracing experiments demonstrated

22

484    that these luminal cells had never expressed Pax8 and thus did not derive from thyrocytes.

485    The second hypothesis was that the cellular stress and loss of tissue homeostasis would recruit

486    macrophages. Indeed, we found that luminal cells were labelled for the conventional

487    macrophage marker, F4/80, are proliferating and display high LAMP-1 signal. In addition, Tg

488    and I-Tg colocalized with the LAMP-1 structures. This observation contributes to explain the

489    colloid exhaustion observed in Vps34$^{cKO}$ and could thus be responsible for the low levels of

490    circulating T$_4$. Although the signal(s) attracting macrophages to the colloid is(are) unknown,

491    the loss of tight junction integrity might facilitate their invasion.

23

506   ***Author disclosures and contributions***

507   BV is a consultant for Karus Therapeutics (Oxford, UK), iOnctura (Geneva, Switzerland) and

508   Venthera (Palo Alto, US) and has received speaker fees from Gilead. The other authors have

509   no competing financial interest. GG and TSW performed the initial morphological and

510   molecular studies and analyzed the data. OD and CS performed all the other experiments

511   and prepared the figures for the revision. VJ and AS participated in data collection and

512   analysis. HGC was involved in supervision of GG. BB and BV provided the Vps34 mice, XHL

513   and SR assayed $T_4$ and TSH levels, and CM provided expertise with $^{125}I$ experiments. PJC and

514   CEP conceived, designed and supervised the project, and wrote the manuscript. All authors

515   have approved the final version of the manuscript.

516   ***Name and address of corresponding author***

517   Prof. Christophe E. Pierreux

518   Cell Biology Unit

519   de Duve Institute and Université Catholique de Louvain

520   75, Avenue Hippocrate

521   B-1200 Brussels

522   Belgium

523   Email: christophe.pierreux@uclouvain.be

524   ***References***

525   1. Colin IM, Denef JF, Lengele B, Many MC, Gerard AC 2013 Recent insights into the cell biology

526        of thyroid angiofollicular units. Endocr Rev 34:209-238.

24

527    2. Carvalho DP, Dupuy C 2017 Thyroid hormone biosynthesis and release. Mol Cell Endocrinol

528        458:6-15.

529    3. Cangul H, Liao X-H, Schoenmakers E, Kero J, Barone S, Srichomkwun P, Iwayama H, Serra

530        EG, Saglam H, Eren E, Tarim O, Nicholas AK, Zvetkova I, Anderson CA, Karet Frankl FE,

531        Boelaert K, Ojaniemi M, Jääskeläinen J, Patyra K, Löf C, Williams ED, UK10K Consortium,

532        Soleimani M, Barrett T, Maher ER, Chatterjee VK, Refetoff S, Schoenmakers N 2018

533        Homozygous loss-of-function mutations in SLC26A7 cause goitrous congenital

534        hypothyroidism. J Clin Ivest Insight 3:e99631.

535    4. Koumarianou P, Gomez-Lopez G, Santisteban P 2017 Pax8 controls thyroid follicular polarity

536        through cadherin-16. J Cell Sci 130:219-231.

537    5. Shivas JM, Morrison HA, Bilder D, Skop AR 2010 Polarity and endocytosis: reciprocal

538        regulation. Trends Cell Biol 20:445-452.

539    6. Rodriguez-Boulan E, Macara IG 2014 Organization and execution of the epithelial polarity

540        programme. Nat Rev Mol Cell Biol 15:225-242.

541    7. Morrison HA, Dionne H, Rusten TE, Brech A, Fisher WW, Pfeiffer BD, Celniker SE, Stenmark

542        H, Bilder D 2008 Regulation of early endosomal entry by the Drosophila tumor

543        suppressors Rabenosyn and Vps45. Mol Biol Cell 19:4167-4176.

544    8. Bilanges B, Posor Y, Vanhaesebroeck B 2019 PI3K isoforms in cell signaling and vesicle

545        trafficking. Nat Rev Mol Cell Biol  May 20. doi: 10.1038/s41580-019-0129-z. [Epub

546        ahead of print].

547    9. Lindmo K, Stenmark H 2006 Regulation of membrane traffic by phosphoinositide 3-kinases.

548        J Cell Sci 119:605-614.

549    10. Juhasz G, Hill JH, Yan Y,Sass M, Baehrecke EH, Backer JM, Neufeld TP 2008 The class III

550          PI(3)K Vps34 promotes autophagy and endocytosis but not TOR signaling in Drosophila.

551          J Cell Biol 181:655-666.

552    11. Backer JM 2008 The regulation and function of Class III PI3Ks: novel roles for Vps34.

553          Biochem J 410:1-17.

554    12. Jaber N, Zong WX 2013 Class III PI3K Vps34: essential roles in autophagy, endocytosis, and

555          heart and liver function. Ann NY Acad Sci 1280:48-51.

556    13. Bechtel W, Helmstädter M, Balica J, Hartleben B, Kiefer B, Hrnjic F, Schell C, Kretz O, Liu S,

557          Geist F, Kerjaschki D, Walz G, Huber TB 2013 Vps34 deficiency reveals the importance

558          of endocytosis for podocyte homeostasis. J Am Soc Nephrol 24:727-743.

559    14. O'Farrell F, Lobert VH, Sneeggen M, Jain A, Katheder NS, Wenzel EM, Schultz SW, Tan KW,

560          Brech A, Stenmark H, Rusten TE 2017 Class III phosphatidylinositol-3-OH kinase

561          controls epithelial integrity through endosomal LKB1 regulation. Nat Cell Biol 19:1412-

562          1423.

563    15. Ronan B, Flamand O, Vescovi L, Dureuil C, Durand L, Fassy F, Bachelot M-F, Lamberton A,

564          Mathieu M, Bertrand T, Marquette J-P, El-Ahmad Y, Filoche-Romme B, Schio L, Garcia-

565          Echeverria C, Goulaouic H, Pasquier B 2014 A highly potent and selective Vps34

566          inhibitor alters vesicle trafficking and autophagy. Nat Chem Biol 10:1013-1019.

567    16. Nascimbeni AC, Codogno P, Morel E 2017 Phosphatidylinositol-3-phosphate in the

568          regulation of autophagy membrane dynamics. FEBS J 284:1267-1278.

569    17. Dupont N, Nascimbeni AC, Morel E, Codogno P 2017 Molecular Mechanisms of

570          Noncanonical Autophagy. Intl Rev Cell Mol Biol 328:1-23.

571    18. Carpentier S, N'Kuli F, Grieco G, Van Der Smissen P, Janssens V, Emonard H, Bilanges B,

572          Vanhaesebroeck B, Gaide Chevronnay HP, Pierreux CE, Tyteca D, Courtoy PJ 2013

573 ClassIII phosphoinositide 3-kinase/VPS34 and dynamin are critical for apical endocytic

574 recycling. Traffic 14:933-948.

575 19. Grieco G, Janssens V, Gaide Chevronnay HP, N'Kuli F, Van Der Smissen P, Wang TS, Shan J,

576 Vainio S, Bilanges B, Jouret F, Vanhaesebroeck B, Pierreux CE, Courtoy PJ 2018

577 Suppression of Vps34 PI 3-kinase activity in kidney proximal tubules abrogates apical

578 trafficking and causes a Fanconi syndrome. Sci Rep 8:14133.

579 20. Shan J, Jokela T, Skovorodkin I, Vainio S 2010 Mapping of the fate of cell lineages generated

580 from cells that express the Wnt4 gene by time-lapse during kidney development.

581 Differentiation 79:57-64.

582 21. Bouchard M, Souabni A, Busslinger M 2004 Tissue-specific expression of cre recombinase

583 from the Pax8 locus. Genesis 38:105-109.

584 22. Valet C, Levade M, Chicanne G, Bilanges B, Cabou C, Viaud J, Gratacap MP, Gaits-Iacovoni

585 F, Vanhaesebroeck B, Payrastre B, Severin S 2017 A dual role for the class III PI3K,

586 Vps34, in platelet production and thrombus growth. Blood 130:2032-2042.

587 23. Pohlenz J, Maqueem A, Cua K, Weiss RE, Van Sande J, Refetoff S 1999 Improved

588 radioimmunoassay for measurement of mouse thyrotropin in serum: strain

589 differences in thyrotropin concentration and thyrotroph sensitivity to thyroid

590 hormone. Thyroid 9:1265-1271.

591 24. Delmarcelle AS, Villacorte M, Hick AC, Pierreux CE 2014 An ex vivo culture system to study

592 thyroid development. J Vis Exp 6:88.

593 25. Hick AC, Delmarcelle AS, Bouquet M, Klotz S, Copetti T, Forez C, Van Der Smissen P,

594 Sonveaux P, Collet JF, Feron O, Courtoy PJ, Pierreux CE 2013 Reciprocal

595 epithelial:endothelial paracrine interactions during thyroid development govern

596 follicular organization and C-cells differentiation. Dev Biol 381:227-240.

27

597    26. Dupasquier S, Delmarcelle AS, Marbaix E, Cosyns JP, Courtoy PJ, Pierreux CE 2014

598        Validation of housekeeping gene and impact on normalized gene expression in clear

599        cell renal cell carcinoma: critical reassessment of YBX3/ZONAB/CSDA expression. BMC

600        Mol Biol 15:9.

601    27. Massart C, Hoste C, Virion A, Ruf J, Dumont JE, Van Sande J 2011 Cell biology of H2O2

602        generation in the thyroid: investigation of the control of dual oxidases (DUOX) activity

603        in intact ex vivo thyroid tissue and cell lines. Mol Cell Endocrinol 343:32-44.

604    28. Zhou X, Takatoh J, Wang F 2011 The mammalian class 3 PI3K (PIK3C3) is required for early

605        embryogenesis and cell proliferation. PloS one 6:e16358.

606    29. Chen J, Chen MX, Fogo AB, Harris RC, Chen JK 2013 mVps34 deletion in podocytes causes

607        glomerulosclerosis by disrupting intracellular vesicle trafficking. J Am Soc Nephrol.

608        24:198-207.

609    30. Bechtel, W, Helmstädter M, Balica J, Hartleben B, Schell C, Huber TB 2013 The class III

610        phosphatidylinositol    3-kinase    PIK3C3/VPS34    regulates    endocytosis    and

611        autophagosome-autolysosome formation in podocytes. Autophagy 9:1097-1099.

612    31. Cohen-Kaplan V, Ciechanover A, Livneh I 2016 p62 at the crossroad of the ubiquitin-

613        proteasome system and autophagy. Oncotarget 7:83833-83834.

614    32. Bjorkoy G, Lamark T, Pankiv S, Overvatn A, Brech A, Johansen T 2009 Monitoring

615        autophagic degradation of p62/SQSTM1. Methods Enzymol 452:181-197.

616    33. Ziros PG, Habeso IG, Chartoumpekis DV, Ntalampyra E, Somm E, Renaud CO, Bongiovanni

617        M, Trougakos IP, Yamamoto M, Kensler TW, Santisteban P, Carrascao N, Ris-Stalpers

618        C, Amendola E, Liao XH, Rossich L, Thomasz L, Juvenal GJ, Refetoff S, Sykiotos GP 2018

619        NFE2-related transcription factor 2 coordinates antioxidant defense with thyroglobulin

620        production and iodination in the thyroid gland. Thyroid 28:780-798.

621    34. Grasberger H, De Deken X, Mayo OB, Raad H, Weiss M, Liao XH, Refetoff S 2012 Mice

622         deficient in dual oxidase maturation factors are severely hypothyroid. Mol Endocrinol

623         26:481-492.

624    35. Christophe-Hobertus C, Christophe D 2010 Delimitation and functional characterization of

625         the bidirectional THOX-DUOXA promoter regions in thyrocytes. Mol Cell Endocrinol

626         317:161-167.

627    36. Twyffels L, Strickaert A, Virreira M, Massart C, Van Sande J, Wauquier C, Beauwens R,

628         Dumont JE, Galietta LJ, Boom A, Kruys V 2014 Anoctamin-1/TMEME16A is the major

629         apical iodide channel of the thyrocyte. Am J Physiol Cell Physiol 307:1102-1112.

630    37. Jaber N, Mohd-Naim N, Wang Z, DeLeon JL, Kim S, Zhong H, Sheshadri N, Dou Z, Edinger

631         AL, Du G, Braga VM, Zong WX 2016 Vps34 regulates Rab7 and late endocytic trafficking

632         through recruitment of the GTPase-activating protein Armus. J Cell Sci 129:4424-4435.

633    38. Gaide Chevronnay HP, Janssens V, Van Der Smissen P, Liao XH, Abid Y, Nevo N, Antignac

634         C, Refetoff S, Cherqui S, Pierreux CE, Courtoy PJ 2015 A mouse model suggests two

635         mechanisms for thyroid alterations in infantile cystinosis: decreased thyroglobulin

636         synthesis due to endoplasmic reticulum stress/unfolded protein response and

637         impaired lysosomal processing. Endocrinology 156:2349-2364.

638    39. Gahl WA, Thoene JG, Schneider JA 2002 Cystinosis. N Engl J Med. 347:111–121.

639    40. Cherqui S, Courtoy PJ 2017 The renal Fanconi syndrome in cystinosis: pathogenic insights

640         and therapeutic perspectives. Nat Rev Nephr 13:115-131.

641    41. Hong Z, Pedersen NM, Wang L, Torgersen ML, Stenmark H, Raiborg C 2017 PtdIns3P

642         controls mTORC1 signaling through lysosomal positioning. J Cell Biol 216:4217-4233.

643    42. Korolchuk VI, Rubinsztein DC 2011 Regulation of autophagy by lysosomal positioning.

644         Autophagy 7:927-928.

29

645 **Figure legends**

646

647 *Figure 1. Genetic and histopathological characterization. A. Extensive genetic excision of*

648 *Vps34 exon 21*. Compared with control (black boxes), Vps34<sup>cKO</sup> thyroid (red boxes) shows ~70%

649 reduction in exon 21 mRNA level at P14. The unchanged mRNA level spanning exons 22-24

650 serves as control. Boxes with median and percentiles of 10 WT and 11 cKO samples; ***, p<

651 0.0001 by Mann-Whitney non-parametric test. *B. Increased thyroid weight.* Compared with

652 control (black boxes), Vps34<sup>cKO</sup> thyroid (red boxes) shows a two-fold increase in thyroid weight.

653 Boxes with median and percentiles of 8 WT and 6 cKO samples; **, p< 0.01 by Mann-Whitney

654 non-parametric test. *C. Histopathological evidence for colloid exhaustion.* As compared to

655 control thyroid tissues (n=3) where all follicles show regular lumen filling with homogenous

656 and intense PAS (Periodic Acid Shiff) staining, Vps34<sup>cKO</sup> thyroids (n=3) present fewer, mostly

657 centrally located, PAS-stained follicles and with weaker staining intensity, other follicles that

658 appear empty (for further quantification, see Supplementary Figure 1). *D. Vps34<sup>cKO</sup> thyrocytes*

659 *are altered and follicles contains abundant non-epithelial cells*. Nuclei are labeled by Hoechst

660 (shown in white); thyrocyte basolateral contours are labeled for E-cadherin (red); two lumen

661 boundaries are delineated by broken lines. As compared to control thyroid follicles, Vps34<sup>cKO</sup>

662 follicular structures are frequently irregular and containing additional cells inside the lumen

663 (arrowheads). These cells are not labeled for E-cadherin.

664

665 *Figure 2. Vps34<sup>cKO</sup> mice display severe hypothyroidism associated with high TSH levels.* As

666 compared to control mice (black boxes), $T_4$ plasma level in Vps34<sup>cKO</sup> is extremely low (red

667 boxes). Conversely, TSH levels are dramatically elevated. (10 WT and 9 cKO samples; ***, p=

668 0.0003 by Mann-Whitney non-parametric test).

30

669    ***Figure 3. Relative expression level of main actors of thyroid hormonogenesis at P14***. Gene

670    expression analysis by RT-qPCR, presented as boxes with median and percentiles. As

671    compared to control thyroid (black boxes), expression in Vps34$^{cKO}$ (red boxes) is preserved for

672    the thyroid-specific genes *Nis*, *Tpo*, *Tg* and *Duox2*. Expression of the TSH receptor (*Tshr*) and

673    of *Slc26a4* is significantly increased in Vps34$^{cKO}$, while expression of *Slc26a7* and *Duoxa2* is

674    significantly decreased. Boxes with median and percentiles of at least 9 control and 9 Vps34$^{cKO}$

675    samples; ***, p< 0.001 by Mann-Whitney non-parametric test.

676

677    ***Figure 4. Normal uptake of iodine but major defect of organification in Vps34$^{cKO}$ thyroid. A.***

678    Comparable $^{125}$I-iodine uptake in the thyroid in control genotypes (black box) and Vps34$^{cKO}$

679    thyroid (red box), but much reduced $^{125}$I bound to protein (in %) in Vps34$^{cKO}$ thyroid,

680    suggesting defective organification. Boxes with median and percentiles of 39 (10 Flox/+, 19

681    Flox/Flox, 10 Cre;Flox/+) and 12 Vps34$^{cKO}$ (Cre;Flox/Flox) samples; ***, p< 0.001 by Mann-

682    Whitney non-parametric test. **B**. Level of $H_2O_2$ in total thyroid extracts show a trend to an

683    increase in Vps34$^{cKO}$ thyroid. Boxes with median and percentiles of 9 control and 9 Vps34$^{cKO}$

684    samples; p= 0.077 by Mann-Whitney non-parametric test.

685

686    ***Figure 5. Normal basolateral but impaired apical organization of tyrocytes. A.*** Thyroid

687    sections from control (left) and Vps34$^{cKO}$ (right) labeled for laminin (red), ezrin (green) and E-

688    cadherin (white). Nuclei are labeled by Hoechst (shown in blue). In control thyroid, laminin

689    surrounds follicles composed of thyrocytes delineated by basolateral E-cadherin and apical

690    ezrin. In Vps34$^{cKO}$, laminin normally surrounds follicles composed of thyrocytes with well-

691    defined basolateral E-cadherin but weaker and less regular apical ezrin. Note here apical

692    membrane bulging in the colloidal space. ***B.*** Thyroid sections from control (left) and Vps34$^{cKO}$

31

693    (right) labeled for ZO-1 (red), Na$^+$/K$^+$-ATPase (green) or β-catenin (white). Nuclei are labeled

694    by Hoechst (shown in blue). In control and Vps34$^{cKO}$ thyroid, Na$^+$/K$^+$-ATPase and β-catenin are

695    correctly localized and restricted to the basolateral pole of the thyrocytes, indicating the

696    presence of a tight junction. However, the tight junction-associated protein ZO-1 is only

697    detected at few apico/basolateral junctions.

698

699    **Figure 6. Evidence for defective iodide organification in Vps34$^{cKO}$ thyroid: follicular lumina**

700    **with Tg but devoid of iodinated-Tg. A.** Thyroid sections from control (left) and Vps34$^{cKO}$ (right)

701    labeled for E-cadherin (green) and thyroglobulin (red), recognized either for a core protein

702    epitope (Tg), or a hormonogenic peptide (I-Tg). Control follicular lumina are round and

703    uniformly labeled for both Tg and I-Tg. In Vps34$^{cKO}$, follicular structures are less regular, with

704    the majority containing Tg, but not the hormonogenic peptide. In Vps34$^{cKO}$, two serial (tilted)

705    sections are shown. **B. Comparison of Tg labelling in control and Vps34$^{cKO}$ thyrocytes.** In control

706    follicles, Tg is essentially restricted to lumen, with little or no signal inside thyrocytes. In

707    Vps34$^{cKO}$, Tg is readily detected within thyrocytes as collections of submicrometric dots or

708    larger spheres (arrowheads). Of note, some luminal cells (broken line in middle panel) also

709    contain Tg-labeled spheres, indicating active endocytosis (arrow).

710

711    **Figure 7. Vps34$^{cKO}$ thyrocytes display increased LAMP-1 signal and impaired I-Tg proteolytic**

712    **processing. A.** Thyroid sections from control (left) and Vps34$^{cKO}$ (right) labeled for

713    thyroglobulin (red), E-cadherin (green) and lysosomal LAMP-1 (white). Nuclei are labeled by

714    Hoechst (shown in blue). In control, thyrocytes rarely contain intracellular Tg and LAMP-1

715    signal is weak. In Vps34$^{cKO}$, most thyrocytes have intracellular Tg (arrowheads) and LAMP-1

716    signal is much increased. Insets show magnification with separate emissions, then merged,

717   channels. Note colocalization of Tg with LAMP-1 in luminal cells (at right). **B.** Thyroid sections

718   from control (left) and Vps34$^{cKO}$ (right) labeled for iodinated-thyroglobulin (I-Tg, red), E-

719   cadherin (green) and lysosomal LAMP-1 (white). Nuclei are labeled by Hoechst (shown in blue).

720   As compared to control follicles which show a weak signal for LAMP-1, and rare intracellular I-

721   Tg, LAMP-1 signal is intense in Vps34$^{cKO}$ thyrocytes and intracellular I-Tg dots are frequently

722   observed (arrowheads). As shown in the enlargements below, LAMP-1-labeled structures in

723   Vps34$^{cKO}$ thyrocytes are enlarged or vacuolated as compared to control.

724

725   ***Figure 8. Vps34$^{cKO}$ thyrocytes show strong accumulation of p62 and LC3b dots.*** **A.** Thyroid

726   sections from control (left) and Vps34$^{cKO}$ (right) labeled for p62 (red), LC3b (green) and

727   lysosomal LAMP-1 (white). Nuclei are labeled by Hoechst (shown in blue). Compared with

728   control follicles, which show low LAMP-1 and almost no signal for p62 and LC3b, all three

729   markers are very strong in Vps34$^{cKO}$ thyroid sections. p62 perfectly co-localizes with LC3b and

730   labels large aggregates. These aggregates are adjacent to LAMP-1-positive structures. **B.**

731   **Increased NRF2 signaling.** Gene expression analysis by RT-qPCR, presented as boxes with

732   median and percentiles. As compared to control thyroid (black boxes), expression of *Nrf2* is

733   reduced in Vps34$^{cKO}$ (red boxes), but level of two out of three NRF2 target genes, *Txnrd1* and

734   *Nqo1* is increased. Boxes with median and percentiles of at least 9 control and 9 Vps34$^{cKO}$

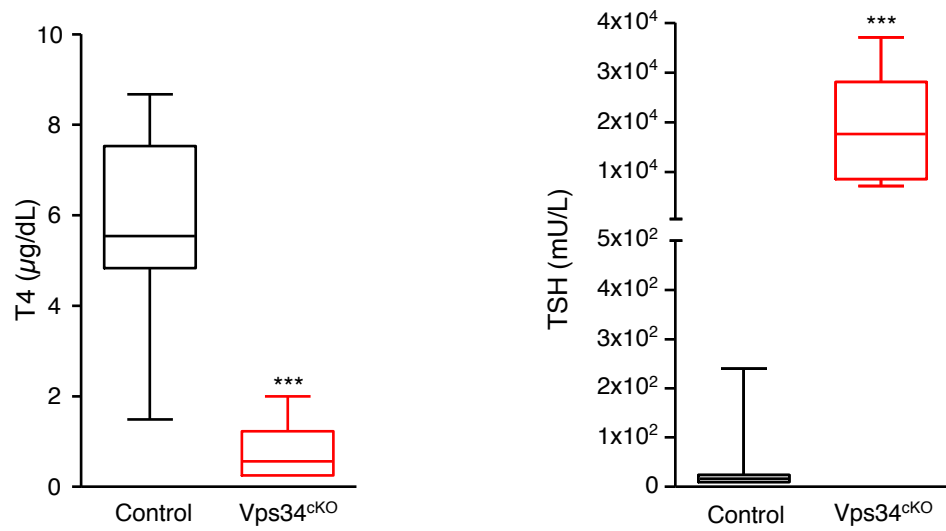735   samples; *, p< 0.05 and ***, p< 0,001 by Mann-Whitney non-parametric test.

736

737   ***Figure 9. Luminal cells in Vps34$^{cKO}$ thyroid are not thyrocytes.*** **A.** Immunolabelling for

738   thyrocyte transcription factor-1 (TTF-1, green); nuclei are visualized with the Hoechst stain

739   (shown in white). In both control and Vps34$^{cKO}$ thyroid, nuclei of thyrocytes circumscribing the

740   follicular lumina are all labeled by the thyrocyte-specific transcription-factor-1, TTF-1. As

741     indicated by the arrowheads, nuclei of luminal cells show no signal for TTF-1 (only white signal

742     representing Hoechst). *B.* Immunolabelling for E-cadherin (red) and YFP (green); nuclei are

743     visualized with the Hoechst stain (shown in blue). Representative images of Vps34cKO thyroid

744     sections reveal expression of YFP only in cells surrounding the follicular lumina, i.e. in cells

745     where Pax8-Cre has been active. Luminal cells do not derive from thyrocyte progenitors as

746     they are negative for YFP.

747

748     *Figure 10. Luminal cells in Vps34$^{cKO}$ thyroid are macrophages.* **A.** Immunolabelling for E-

749     cadherin (red), and for the conventional macrophage marker (F4/80, green); nuclei are

750     visualized with the Hoechst stain (shown in white). In Vps34$^{cKO}$ thyroid, F4/80 signal can be

751     found in the interstitium (arrows), but also in the colloidal space, thus identifying luminal cells

752     as infiltrating macrophages. **D. Luminal cells are taking up the colloid.** Immunolabelling for I-

753     Tg (red), F4/80 (green) and LAMP-1 (white). Nuclei are visualized with the Hoechst stain

754     (shown in blue). Luminal cells in Vps34$^{cKO}$ have abundant LAMP-1 structures that surround I-Tg

755     droplets. Arrowheads show additional I-Tg in thyrocytes. Broken lines indicate luminal
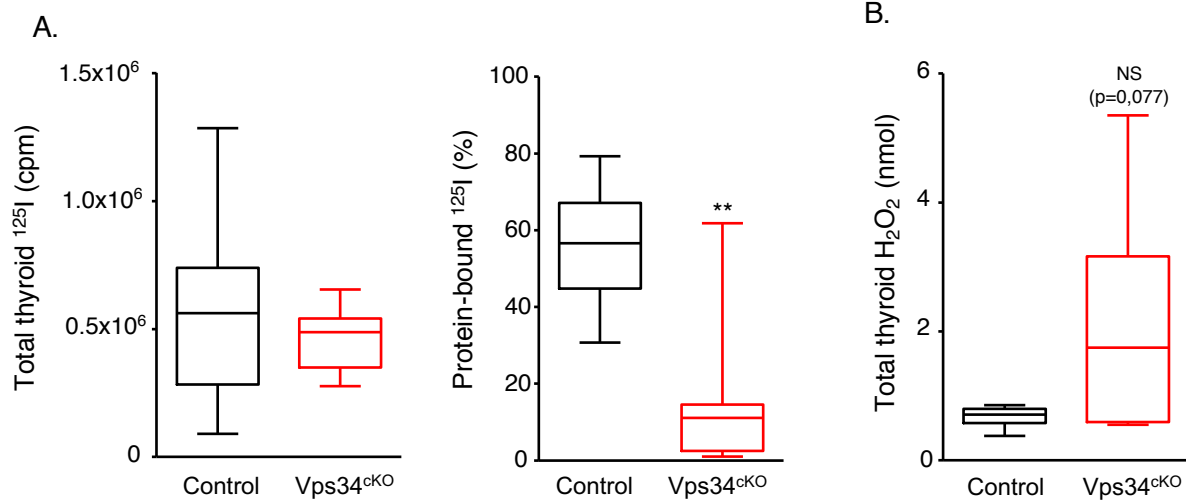
756     contours.
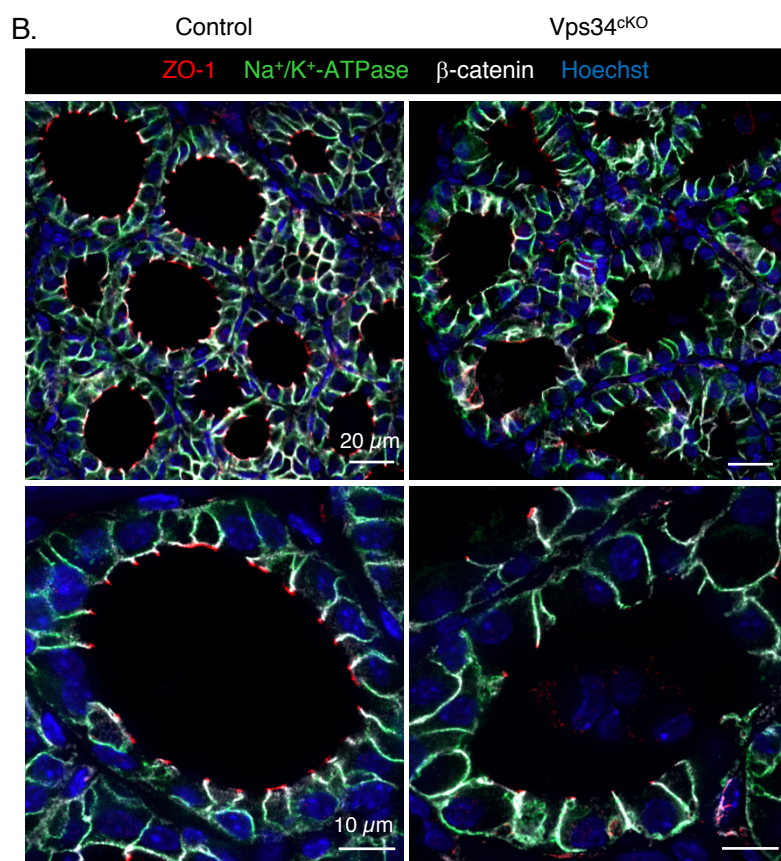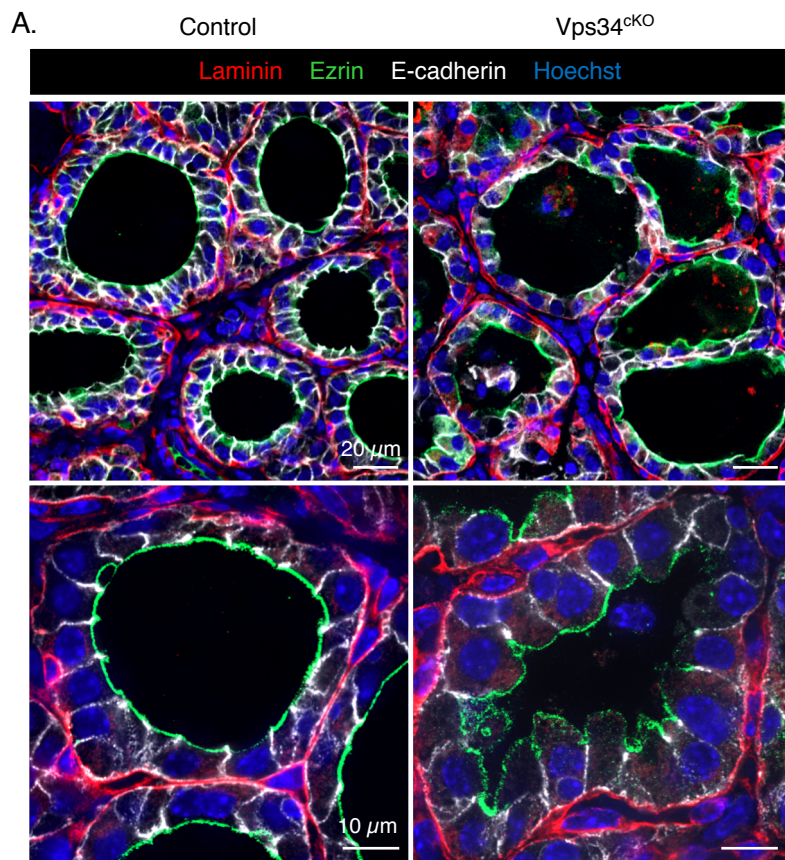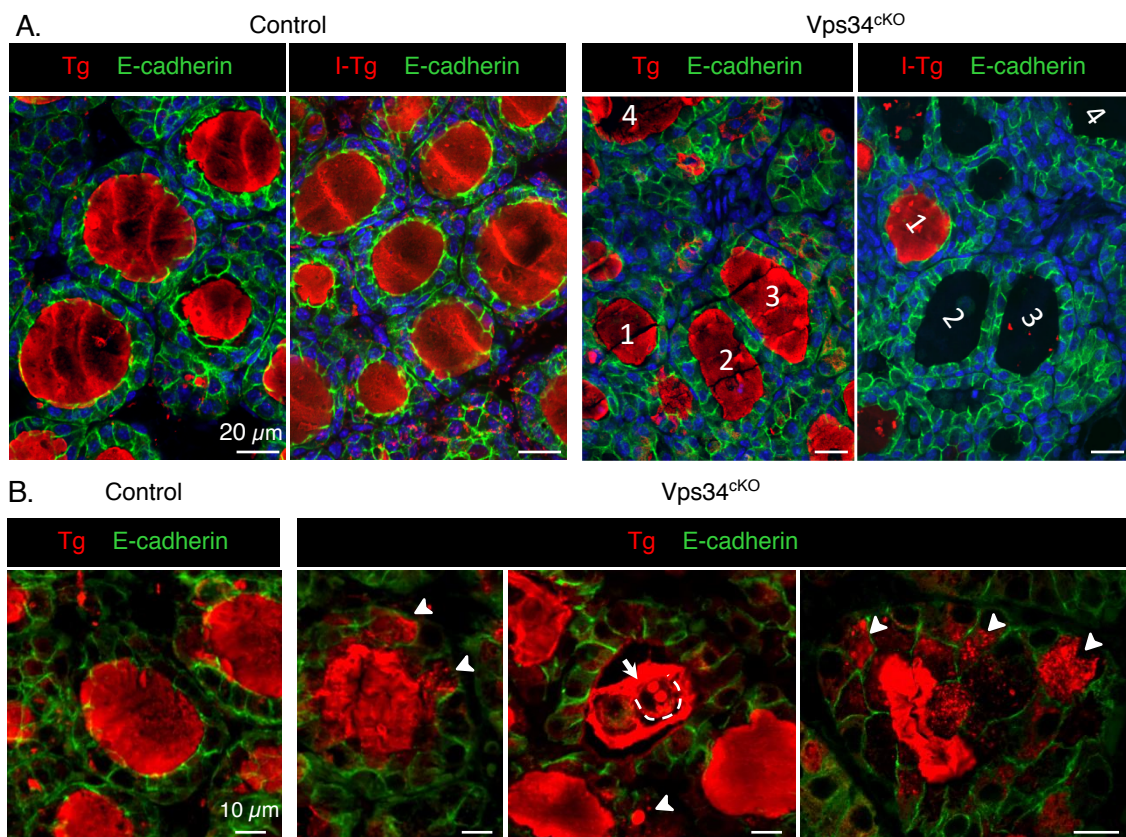
757

**A.**

Relative expression

Control · Vps34^cKO

ex20-21 ***  ex21-22 ***  ex22-24

**B.**

Thyroid weight (mg)

Control · Vps34^cKO **

**C.**

Control: #1, #2, #3 (200 μm)

Vps34^cKO: #1 (200 μm), #2, #3

**D.**

Control · Vps34^cKO

E-cadherin Hoechst

10 μm

GriecoFig1

GriecoFig2

GriecoFig3

A.

Total thyroid $^{125}$I (cpm)

Protein-bound $^{125}$I (%)

**

Control    Vps34$^{cKO}$

B.

Total thyroid $H_2O_2$ (nmol)

NS
(p=0,077)

Control    Vps34$^{cKO}$

GriecoFig4

A.

Control | Vps34<sup>cKO</sup>

Laminin  Ezrin  E-cadherin  Hoechst

20 μm

10 μm

B.

Control | Vps34<sup>cKO</sup>

ZO-1  Na⁺/K⁺-ATPase  β-catenin  Hoechst

20 μm

10 μm

GriecoFig5

A. Control | Vps34^cKO

Tg  E-cadherin    I-Tg  E-cadherin    Tg  E-cadherin    I-Tg  E-cadherin

B. Control | Vps34^cKO

Tg  E-cadherin    Tg  E-cadherin

20 μm

10 μm

GriecoFig6

A.

Control | Vps34^cKO

Tg  E-cadherin  LAMP-1  Hoechst

10 μm

2,5 μm

Tg | E-cadherin | LAMP-1 | Merge

B.

Control | Vps34^cKO

I-Tg  E-cadherin  LAMP-1  Hoechst

10 μm

2,5 μm

I-Tg | E-cadherin | LAMP-1 | Merge

GriecoFig7

**A.** Control / Vps34^cKO — p62 LC3b LAMP-1 Hoechst; 10 μm

**B.** Relative expression for Nrf2, Txnrd1, Nqo1, Gpx2 (Control vs Vps34^cKO)

GriecoFig8

A. Control Vps34^cKO

TTF-1 Hoechst

20 µm

B. Vps34^cKO

E-cadherin YFP Hoechst

20 µm

GriecoFig9

A. Vps34cKO

E-cadherin  F4/80  Hoechst

10 μm

B. Vps34cKO

I-Tg  F4/80  LAMP-1  Hoechst

10 μm

| I-Tg | F4/80 | LAMP-1 | Merge |

5 μm

| I-Tg | F4/80 | LAMP-1 | Merge |

GriecoFig10